Mechanical properties of elementary layers involved in a multilayer optical stack by photon-acoustic phonon interaction approaches

Frédéric Faëse, Delphine Poinot Cherroret, Sébastien Chatel, Loic Becerra, Fatiha Challali, Philippe Djemia, Laurent Belliard

JOURNAL OF APPLIED PHYSICS **124**, 125307 (2018)

Mechanical properties of elementary layers involved in a multilayer optical stack by photon-acoustic phonon interaction approaches

Frédéric Faëse,[1,a)] Delphine Poinot Cherroret,[2] Sébastien Chatel,[2] Loic Becerra,[1] Fatiha Challali,[3] Philippe Djemia,[3] and Laurent Belliard[1]
[1]*Institut des NanoSciences de Paris, UMR 7588, CNRS, UPMC, 4 place Jussieu, Paris 75005, France*
[2]*Essilor International, R&D, 81 Boulevard Jean-Baptiste Oudry, 94000 Créteil, France*
[3]*Université Paris 13, Sorbonne Paris Cité, Laboratoire des Sciences des Procédés et des Matériaux, CNRS, F-93430 Villetaneuse, France*

(Received 25 March 2018; accepted 2 September 2018; published online 26 September 2018)

Two complementary techniques, picosecond ultrasonics (PU) and Brillouin light scattering (BLS), have been performed to measure the mechanical properties of layers involved in an optical stack. One of the advantages of these two techniques is their ability to analyze samples whose thickness varies from a few tens of nanometers (the anti-reflective coating) to several millimeters (the polymer substrate). Since all the layers constituting the optical stack have proved to be isotropic, they are completely elastically characterized thanks to the two techniques. Moreover, as the two independent elastic coefficients are measured by PU and BLS, c_{33} and c_{44}, respectively, the complete stiffness matrix and, hence, the Poisson's ratio and the Young's modulus can be deduced. *Published by AIP Publishing.* https://doi.org/10.1063/1.5030749

I. INTRODUCTION

Optical thin films are used in many fields: ophthalmic lenses, optronics, screens, architectural glasses, photovoltaics, etc. These systems are subject to various mechanical solicitations during their lifetime.[1,2] Thus, when designing such optical systems, it is also important to take into account their mechanical behavior regarding fracture and tribological issues. That can be achieved by combining experimental characterizations and analysis by finite element simulations.[3] In all cases, basic physico-mechanical properties of materials involved in these systems such as density, Young's modulus, physical thickness, residual stress, Poisson's ratio, and toughness must be first measured accurately.

The mechanical properties characterization of these systems is, therefore, essential and presents several technical and scientific issues.

For example, the Young's modulus can be measured by nanoindentation,[4] but this technique remains problematic for characterizing very thin layers or multilayer systems.[5] In addition, the influence of the substrate may not be overcome, in particular, in the case of stiff thin films deposited on very compliant substrates.[6] Other techniques can be used such as bulge tests, buckling-based metrology, or resonant methods[7] but each of these techniques presents some material and experimental limitations. This present work focuses on the example of ophthalmic lenses. The latter consist of thin optical layers deposited on a polymer substrate being either a thermoset or a thermoplastic polymer with a thickness in the mm range. These polymer substrates offer a higher refractive index and are lighter than mineral glasses, but they are unfortunately more scratch sensitive. To overcome this weakness, a polymer composite hardcoat a few microns thick is deposited onto the substrate before applying thin optical layers. Such a system, therefore, combines materials having various thicknesses and mechanical properties that make it challenging to characterize.

This study investigates elastic characterization in elementary layer by combining picosecond ultrasonics (PU) and Brillouin light scattering (BLS) techniques, as already reported in low-k dielectric material.[8] BLS has also been successfully applied to measure the longitudinal elastic modulus in crystalline lens in the eye, first and so crucial element in the formation of images.[9]

II. SAMPLES AND EXPERIMENTAL SETUPS

A. Samples preparation

An example of optical multilayer system used in this study is presented in Fig. 1.

It encompasses SiO_2 and ZrO_2 optical thin films deposited on top of a 4.5 μm composite polymer, referred to as a hardcoat, on a 2 mm thick CR39® polymer substrate commonly used in the ophthalmic industry whose optical index is 1.5. The composite hardcoat is itself composed of an anti-shock layer and of an anti-abrasion layer, deposited in this order on the substrate. Each of these materials was also deposited as a single layer on a silicon wafer (in the case of SiO_2 and ZrO_2 thin films) or on a silicon wafer coated with a 100 nm thick Ti layer (in the case of anti-abrasion layer, anti-shock layer, and composite hardcoat) as model materials. The composite hardcoat was made by dip coating according to the procedure described in Ref. 10. SiO_2 and ZrO_2 thin films were deposited in a Balzers BAK 760 coating machine by electron beam evaporated at ambient temperature (20-30 °C), using the same procedure as Roisin *et al.*[11] The substrate holder was rotated continuously during the deposition

a)Author to whom correspondence should be addressed: faese.frederic@orange.fr. Tel.: +33 6 68 44 31 08.

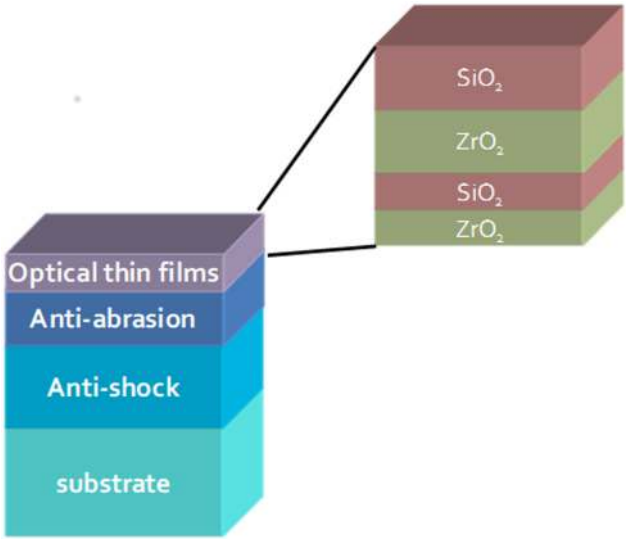

FIG. 1. Example of an ophthalmic lens (the thickness of the different layers is not represented at scale).

process. SiO_2 layers were deposited without reactive gas under base pressure, whereas ZrO_2 layers were deposited using two processes named A and B. In A process, ZrO_2 thin films were deposited along with O_2 gas and the working pressure was in the 10^{-5} mbar range. In B process, ZrO_2 thin films were deposited by electron beam evaporation assisted by O_2 ion beam using an End-Hall Ion Source (Mark II) and the working pressure was in the 10^{-4} mbar range. Deposition rate was 0.3 nm/s (ZrO_2) and 1 nm/s (SiO_2) and was controlled during deposition by using Quartz Crystal Microbalance monitoring. The thickness and the optical properties of these coatings were measured by spectroscopic ellipsometry (thanks to a VASE ellipsometer, J.A. Woolam Company, Inc.), whereas the density and the thickness were complementarily measured by XRR experiments (X-Ray Reflectivity). An estimated porosity fraction was deduced from measured density. Some nanoindentation experiments were also performed on monolayers using an MTS XP apparatus with a Berkovich diamond tip. The nanoindentation results have been calculated following the Oliver & Pharr method.[4]

B. Experimental setups

1. Picosecond ultrasonics

Time resolved measurements were performed using a standard picosecond ultrasonic setup.[12–14] The pump and probe beams, emitted simultaneously by a mode-locked Ti:Sapphire Tsunami Spectra-Physics laser source operating at 800 nm with a repetition rate around 79.3 MHz, are focused by means of a long working distance lens on aluminum or titanium thin film transducers. Following the modulated pump absorption, an ultrafast lattice deformation is induced, creating a coherent acoustic pulse at the free surface. This longitudinal acoustic wave propagating normal to the sample surface is partly transmitted and reflected back at various interfaces and finally detected through the transient sample reflectivity at the free surface using a time delayed probe beam.

In layers more than 80 nm thick, knowing the sample thickness and measuring the time of flight in the stacking, the longitudinal sound velocity of the different layers could be obtained. In the case of films with a thickness lower than 80 nm, in which the different echo signatures may overlap, the experimental transient sample reflectivity is compared and adjusted according to a standard approach based on one-dimensional elastic model including the transfer-matrix formalism. This formalism is well adequate to the calculation of the acoustic wave propagation in layered structures.[15]

When the layer is several microns thick, the echoes are often too much attenuated to be detected after a round trip. Nevertheless, the longitudinal velocity could be extracted in transparent materials thanks to the Brillouin oscillations.[16] These oscillations are due to the interference between the probe beams partly reflected on the free surface and on the acoustic wavefront that propagates inside the layer. As the probe beam is focused by a long working distance lens, low incident angles are to be considered. In that case, the Brillouin frequency f_B is given by

$$f_B = \frac{2nV_l}{\lambda_0}, \tag{1}$$

where λ_0 is the probe laser wavelength in vacuum, n the layer optical index at λ_0, and V_l the longitudinal sound velocity in the layer.

2. Brillouin light scattering

Brillouin inelastic light scattering (wave vector $\boldsymbol{k_S}$ and frequency f_S) was analyzed by means of a Sandercock-type 3 + 3 pass tandem Fabry-Perot interferometer, in the backscattering geometry considering two possibilities for the coupling of the incoming light (wave vector $\boldsymbol{k_I}$ and frequency f_I) with the acoustic waves (wave vector $\boldsymbol{Q}$ and frequency f) (see Fig. 2) satisfying $\boldsymbol{k_S} = -\boldsymbol{k_I}$, $\boldsymbol{k_S} - \boldsymbol{k_I} = \pm\boldsymbol{Q}$ and $f_S - f_I = \pm f$. Firstly, one can consider the bulk acoustic waves (BAW) traveling nearly perpendicular to the film plane with a wave vector direction ($\boldsymbol{Q_1}$) that makes an angle α [$sin(\alpha) = sin(\theta)/n$,

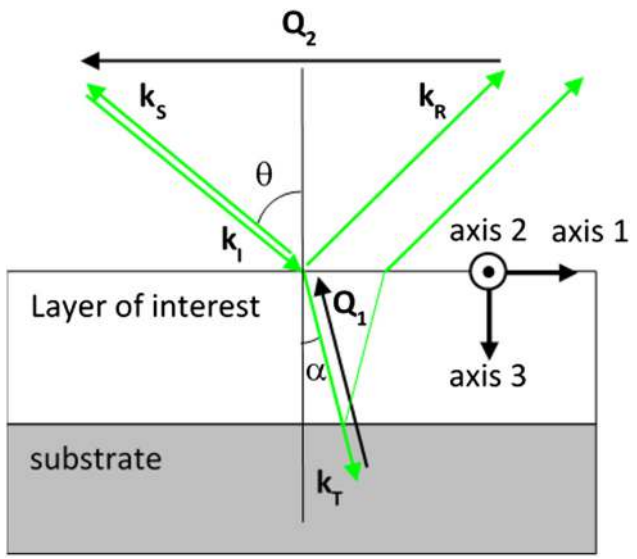

FIG. 2. Brillouin Light Scattering principle.

n is the refractive index of the film and θ the angle of incidence of the light] with the perpendicular z-axis, and a wave vector modulus $Q_1 = 4\pi n/\lambda_L$, λ_L is the wavelength of the incident laser beam (532 nm). Secondly, one can consider BAW and the surface acoustic waves (SAW) propagating along one in-plane direction with a wave vector direction ($\boldsymbol{Q_2}$) and with a wave vector modulus $Q_2 = 4\pi sin(\theta)/\lambda_L$.

Considering BAW, the active mechanism is the photoelastic coupling within the transparent thick film.[17] It is fully efficient in the case of the thick resins samples deposited on a silicon substrate. We can observe longitudinal acoustic wave propagating out of the plane with frequency (f) and sound wave velocity (V_L) related by $V_{L1} = 2\pi.f_1/Q_1$ or propagating along one in-plane direction with $V_{L2} = 2\pi f_2/Q_2$.

In the case of a "slow" film on a "fast" substrate ($V_T^{Film} < V_T^{Substrate}$), both the Rayleigh surface wave (R) and the Sezawa standing waves (S_i) can be observed.[18–20] Frequencies (f) and sound wave velocities (V_{SAW}) are related by $V_{SAW} = 2\pi f/Q_2$. For thin films (thickness $t < 2\pi/Q_2$), V_{SAW} are dispersive as a function of $(Q_2 t)$. Two different set of samples have been considered: SiO_2 and ZrO_2 thin films on a silicon substrate with a 20 nm Ti or Al cap layer and without a cap layer. The addition of the thin metal layer, called opacifier, enabled faster acquisition of spectra enhancing the visibility of the Rayleigh surface wave lying at the lowest frequency and with the highest intensity. The BLS spectra were obtained at room temperature with a typical counting time of 1 h for samples with a cap layer and 12 h without a cap layer. All spectra obtained for different θ in the range [45°, 75°] were fitted by considering the dynamical corrugation [$u_z(\omega = 2\pi f,\ z = 0)$ where f is the frequency and u_z the vertical atomic displacement] at the free surface and at the (metal oxide)/Si interface, as being the active ripple mechanism responsible for inelastic light scattering.[20,21] Input parameters are the elastic properties, the mass density, and thickness of all constituents of the stack. For the thin films, the c_{33} elastic constant of the film is considered fixed to the one measured by PU while the remaining independent c_{44} elastic constant has to be determined. Isotropic elastic properties of the polycrystalline Ti and Al cap layers have been previously determined on thicker films, combining picosecond ultrasonics and BLS measurements.[22]

C. Complete material characterization

The axes corresponding to the indexes of the elastic coefficients are the ones represented in Fig. 2.

As it is mentioned in Sec. II B 1, the PU setup gives a direct access to the longitudinal velocity V_l of the acoustic waves propagating in the layer of interest. Hence, knowing the density of the layer ρ, the value of the elastic coefficient c_{33} is determined thanks to the following relation: $c_{33} = \rho V_l^2$.

Similarly, Sec. II B 2 illustrates how the BLS setup gives the value of the elastic coefficient in the layer of interest c_{44} (related to the value of the transverse velocity V_t of the acoustic waves: $c_{44} = \rho V_t^2$).

As the density has been measured by XRR, the elasticity of isotropic material is completely included in these two elastic constants giving access to the Young's modulus E and the Poison's ratio v:

$$E = c_{44}\frac{3c_{11} - 4c_{44}}{c_{11} - c_{44}}, \tag{2}$$

$$v = \frac{c_{11} - 2c_{44}}{2(c_{11} - c_{44})}. \tag{3}$$

III. RESULTS AND DISCUSSION

A. Single layer characterization

First, the CR39© polymer substrate, support of the entire optical stacking, plays the role of optical correction for the spectacles holder. Moreover, as the substrate is about one millimeter thick, the volume measurement of its mechanical characteristics without opacifier is relevant with the BLS setup. The PU approach is in general more relevant in thinner films, which explains that only the BLS approach has been used in the CR39© substrate.

Figure 3 illustrates a standard BLS spectrum measured on an uncoated CR39© substrate showing the frequency f_1 of a bulk longitudinal wave such as $V_{L1} = 2\pi f_1/Q_1$. A similar spectrum is measured when the CR39© substrate is covered by a thin Ti cap layer, giving the value of V_t thanks to a numerical model[23] that fits the Rayleigh surface wave line at lower frequency.

The substrate studied here is a CR39© viscoelastic substrate, i.e., an organic substrate whose optical index is 1.5. Its mechanical characteristics measured at a frequency close to 15 GHz are a longitudinal velocity $(V_l)_{CR39©} = 2.87 \pm 0.10\ nm/ps$; a transverse velocity $(V_t)_{CR39©} = 1.35 \pm 0.08\ nm/ps$; a Young's modulus $E_{CR39©} = 6.52 \pm 0.30\ GPa$; and a Poisson's ratio $v_{CR39©} = 0.36 \pm 0.03$.

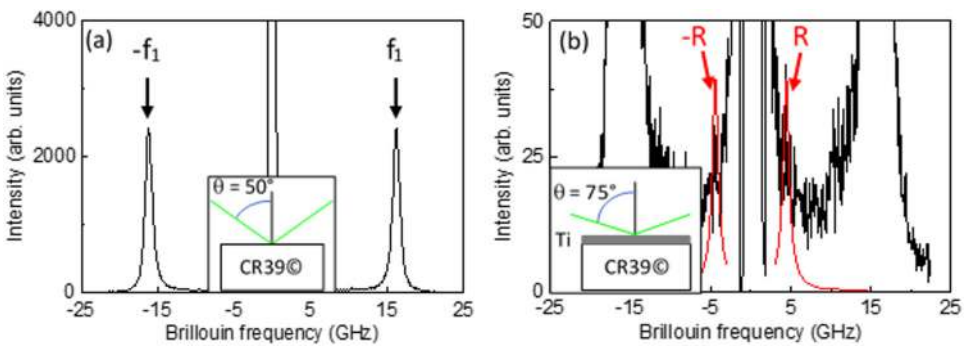

FIG. 3. Standard BLS spectrum measured on a CR39© substrate for an angle of incidence $\theta = 50°$ (a). BLS spectrum on the same substrate covered by a 20 nm titanium cap layer for an angle of incidence $\theta = 75°$ (in black: experimental results; in red: simulation results of the Rayleigh surface wave) (b). f_1 and R denote the bulk longitudinal wave and the Rayleigh surface wave, respectively. Insets: schematic diagram of the experimental geometry.

These results have to be compared with the quasi-static measurement of the Young's modulus obtained by Essilor thanks to nanoindentation: $(E_{CR39©})_{nano} \approx 2.8\ GPa$. The difference between these results on a viscoelastic material obtained with the acoustical methods and nanoindentation could be explained by the large frequency difference of the measurement technique: in our study, acoustical phenomena occur at a frequency of several GHz, whereas nanoindentation measures phenomena whose frequency is around 80 Hz (quasi-static). This frequency dependence hypothesis is suggested by an apparent softening of the Young's modulus sample when the measurement frequency is decreased. That is equivalent to an increase of the temperature,[24,25] leading generally to a softening.

The layer in contact with the previous substrate is the hard coating, containing two complementary layers: the anti-shock layer, near the substrate, and the anti-abrasion layer. For further details on this hard coating, refer to the Essilor patent (Ref. 10). Each layer of the hard coating, as well as the two layers together, has been studied thanks to the PU setup and the BLS setup. As for the substrate, the hard coating is a poor thermal conductor. Nevertheless, a PU study is possible because the samples have been prepared by dip coating of the layer(s) on a silicon wafer previously covered by a 100 nm thick titanium transducer. As the transducer is in contact with the silicon wafer, the heat deposited by the laser is efficiently dissipated within the wafer.

Figure 4 illustrates a standard PU signature measured on the hard coating showing Brillouin oscillations, whose frequency f_B is related to the longitudinal velocity following Eq. (1). Complementarily, BLS gives another estimate of the longitudinal velocity and allows a determination of the transverse velocity. Due to the different wavelength used in BLS ($\lambda_{BLS} = 532$ nm) and PU ($\lambda_{PU} = 800$ nm), the frequency of the bulk longitudinal acoustic wave involved in both experiments

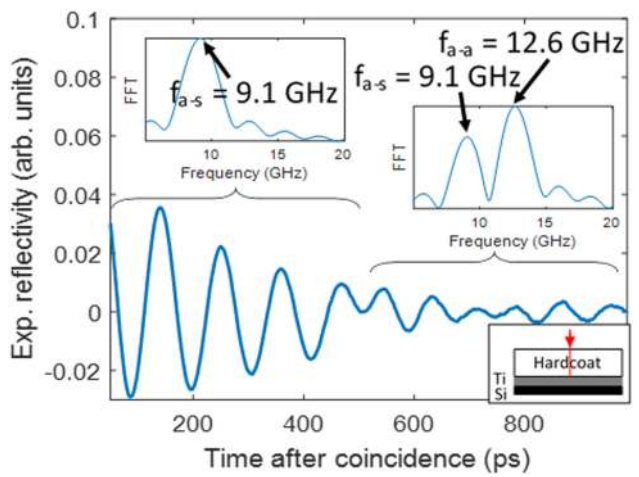

FIG. 4. Experimental reflectivity measured on the hard coating and Fourier transform of the signal before and after 500 ps (upper insets); schematic diagram of the experimental geometry (lower inset). Before around 500 ps, the Brillouin oscillations occur in the anti-shock layer alone with a frequency $f_{a\text{-}s} = 9$ GHz; after 500 ps, the Brillouin oscillations occur in both the anti-shock and the anti-abrasion layers, giving the frequencies $f_{a\text{-}s} = 9.1$ GHz and $f_{a\text{-}a} = 12.6$ GHz, respectively, as the acoustic wavefront has been partially reflected and transmitted at the anti-shock layer/anti-abrasion layer interface.

is slightly different [it scales with $\sim n/\lambda$, see Eq. (1)] being necessarily higher for BLS than for PU (relative difference is ~33%). Considering errors for both experiments, sound velocities have remained very close but with longitudinal sound velocity measured by BLS, systematically slightly higher than the one measured by PU (see Table I).

The anti-shock layer and the anti-abrasion layer have first been investigated alone. Then, the two layers have been studied together to investigate possible mutual interaction. Experimental results used to calculate the longitudinal velocities with the PU setup and with the BLS setup are shown in Figs. 4 and 5, respectively. Let us mention that, regarding the anti-shock layer of the hard coating, the transverse velocity (and consequently the Young's modulus and the Poisson's ratio) could not be measured as this layer is buried. The values on the anti-shock layer alone and on the anti-shock layer composing the hard coating are the same if we take into account the measurement uncertainty. The conclusion is the same for the anti-abrasion layer, even if the anti-abrasion layer composing the hard coating seems to show slightly higher values in velocity (≈+5%) and Young's modulus (+6%) than the anti-abrasion layer alone. This hardening is not significant and can be due to different deposition conditions.

As previously, the values in Table I can be compared with the ones obtained with the nanoindentation method: $(E_{a\text{-}a})_{alone} = 4.5 \pm 0.5\ GPa$ and $(E_{a\text{-}a})_{HC} = 5.0 \pm 1.0\ GPa$ concerning the anti-abrasion layer (index a-a) alone and the anti-abrasion layer of the hard coating (HC), respectively. Once again, the sample proves to be harder when the frequency of the measurement increases (acoustical methods compared to the nanoindentation method).

On an optical stack, the layer deposited on the hard coating is the anti-reflective one which is made up of a series of thin metal oxide layers. As far as we are concerned, the two materials of interest are zirconia and silica. We have thus studied by PU and BLS, two typical layers of each of these materials, both around 80 nm thick for the echoes to be easily identified with the PU setup. Figure 6 shows two longitudinal acoustic features, corresponding to one and two round trips in the zirconia sample film, allowing to measure the time of flight of the acoustic wave propagating on the sample. The longitudinal velocity is easily calculated knowing the sample thickness. On the one hand, the results for the zirconia are the following ones: a longitudinal velocity $(V_l)_{ZrO2} = 5.80 \pm 0.10\ nm/ps$ deduced from PU measurements; a transverse velocity $(V_t)_{ZrO2} = 3.13 \pm 0.08\ nm/ps$ *obtained by BLS*; a Young's modulus $E_{ZrO2} = 124.28 \pm 4.42\ GPa$; and a Poisson's ratio $\nu_{ZrO2} = 0.29 \pm 0.02$.

These values are relatively in good agreement with a previous work on bulk porous zirconia ceramics[26] considering the measured 10% porosity fraction. The reference Young's modulus and Poisson's ratio for the dense ZrO_2 ceramic material are 209 GPa and 0.31, respectively.

On the other hand, the results for the silica are the following: a longitudinal velocity $(V_l)_{SiO2} = 5.00 \pm 0.10\ nm/ps$; a transverse velocity $(V_t)_{SiO2} = 3.01 \pm 0.12\ nm/ps$; a Young's modulus $E_{SiO2} = 46.22 \pm 2.36\ GPa$; and a Poisson's ratio $\nu_{SiO2} = 0.22 \pm 0.05$.

TABLE I. High frequency mechanical characteristics of the viscoelastic layers constituting the hard coating. We can notice that the longitudinal sound velocity extracted from PU and BLS are very close but $V_L(\text{BLS}) \geq V_L(\text{PU})$ within respective uncertainties.

Layer	Longitudinal velocity measured by PU (nm/ps)	Longitudinal velocity measured by BLS (nm/ps)	Transverse velocity (nm/ps)	Young's modulus (GPa)	Poisson's ratio
Anti-shock layer alone	2.40 ± 0.13	2.54 ± 0.05	1.16 ± 0.06	5.75 ± 0.23	0.37 ± 0.02
Anti-abrasion layer alone	3.26 ± 0.14	3.35 ± 0.04	1.91 ± 0.09	14.35 ± 0.67	0.26 ± 0.04
Anti-shock layer of the hard coating	2.45 ± 0.13	2.59 ± 0.04	N/A	N/A	N/A
Anti-abrasion layer of the hard coating	3.42 ± 0.13	3.49 ± 0.03	1.96 ± 0.10	15.23 ± 0.68	0.27 ± 0.04

The Young's modulus and the Poisson's ratio of our evaporated SiO_2 thin films are, respectively, lower and higher, than the values for dense silica ($E \sim 72$ GPa and $\nu = 0.16$) reported in the literature[27,28] on thicker films (220-600 nm) deposited by plasma enhanced chemical vapor deposition or radio frequency sputtering on a (100) silicon substrate. Such a discrepancy (−36%) could be related to the different elaboration processes and deposition temperature resulting to a much higher porosity fraction (10% in this case) and size of pores for the evaporated samples. Nonetheless, the lowering of the Si-O bond strength due to a change in their interatomic distance and the modification of Si-O-Si bridging bond angle are also other possibilities.[29]

B. Deeper study of the zirconia layer

The motivation to investigate both elastic anisotropy/isotropy and thickness dependence is justified by two reasons:

- First, in an industrial final product, the reflection coating is composed of several layers with thicknesses ranging from 80 nm to 20 nm. Obviously, the elastic response with variable thicknesses is a relevant information needed to further perform mechanical simulations.
- Second, the question of isotropic or anisotropic elastic properties arises following TEM investigations performed in the cross section which have demonstrated microstructural anisotropy due to a columnar growth and porosities that can affect the elastic constants by its shape and the concentration.

1. Isotropy

In order to test the isotropy assumption of the zirconia, two samples have been deposited following the two main processes: process A and process B (see Sec. II A). A first series of measurements aims at determining the zirconia isotropy in the in-plane geometry by measuring the Brillouin spectra with a fixed incidence angle ($\theta = 65°$) and for different in-plane angles φ [see Fig. 7(a)]. Considering the steadiness of the experimental results [see Fig. 7(b)], the zirconia samples are proved to be isotropic in the in-plane geometry.

In order to determine the zirconia isotropy in the out-of-plane geometry, Brillouin spectra and the associated simulations have been obtained for different values of the incidence angle θ, with and without opacifier. For both processes of deposition, the experimental results and the simulations are in very good agreement, whatever the incidence angle, the sample being metalized or not. If we consider, first, that the simulations have been performed by taking into account the value of the elastic coefficient c_{33} (out-of-plane) measured with the PU setup and, second, that the observed Sezawa mode position can be affected by the elastic coefficients $c_{11} = c_{22} \neq c_{33}$ (in-plane), the simulations accuracy

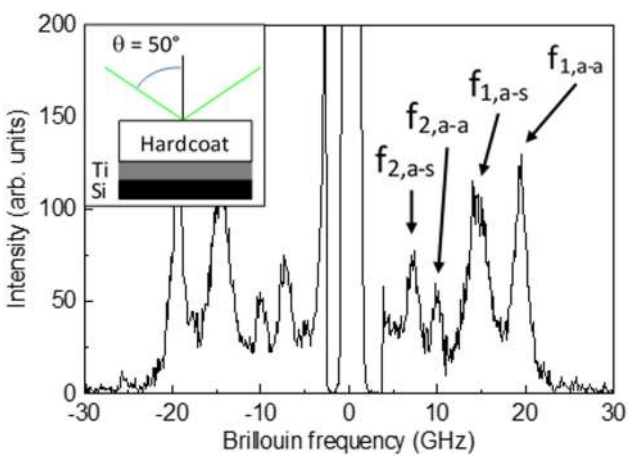

FIG. 5. Brillouin spectrum measured on the hard coating at an angle $\theta = 50°$; schematic diagram of the experimental geometry (inset). Four frequencies are clearly visible, corresponding to the out-of-plane geometry $\mathbf{Q}_1$ (index 1) and the in-plane geometry $\mathbf{Q}_2$ (index 2) for each of the layer constituting the hard coating: the anti-shock layer, index a-s, and the anti-abrasion layer, index a-a.

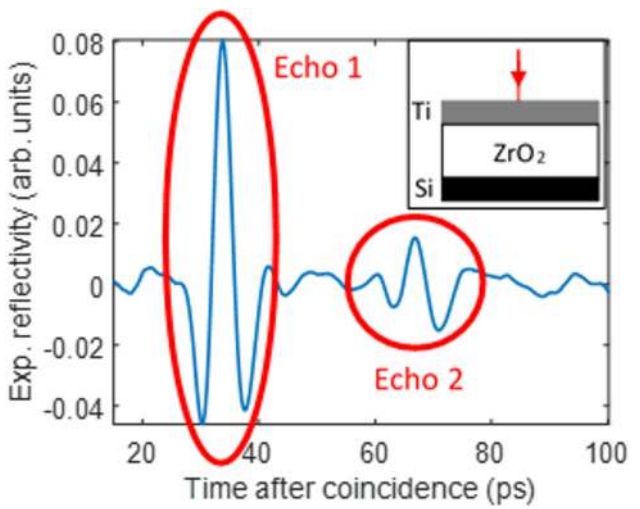

FIG. 6. Experimental reflectivity showing two echoes on a Process A zirconia sample 80 nm thick; schematic diagram of the experimental geometry (inset).

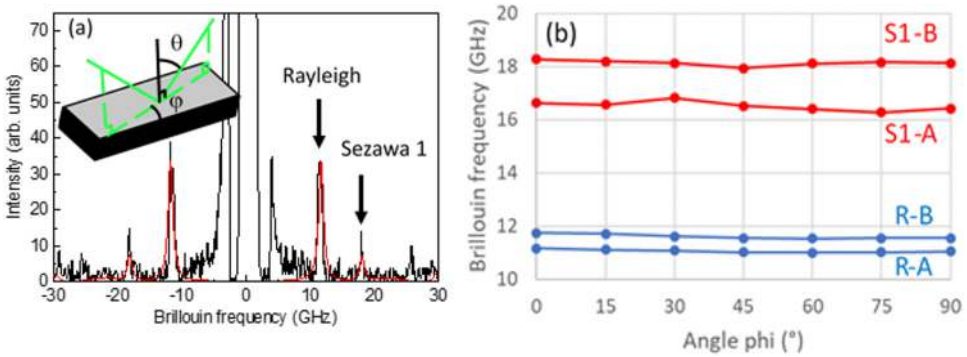

FIG. 7. Typical Brillouin spectrum obtained for an angle $\theta = 65°$ showing the Rayleigh mode and the first Sezawa mode (in black: experimental results; in red: simulation results); in the inset, schematic principle of measurement of the in-plane isotropy (a). Frequency of the Rayleigh mode (R) and of the first Sezawa mode (S1) for the zirconia samples deposited following processes A and B for different in plane angles (b).

implies that the zirconia samples can be considered as being elastically isotropic in the in-plane and in the out-of-plane geometries. As it can be seen in Fig. 7(b), the discrepancy between the Brillouin frequencies related to process A and process B showing that process B samples are harder than process A samples may be due to a difference in the sample microstructure.

2. *Effect of the thickness*

A series of zirconia samples have been deposited on silicon wafers following the B process. Their thickness varies from about 20 nm to about 90 nm with a 10 nm step. Their mechanical characteristics have been measured thanks to the two experimental setups and are shown in Fig. 8.

Regarding the measurement uncertainty shown in Fig. 8, the results obtained for the two lowest thicknesses prove to be relatively imprecise, especially concerning the Young's modulus and the Poisson's ratio. Further studies are still needed to elucidate the elastic behavior of these films with thicknesses less than 30 nm and the possible correlations with the microstructure. New specific tools have to be designed for such an ambitious goal, as exemplary in the work of Hernandez-Charpak *et al.*,[30] who developed a new ultrasonic setup to generate high frequency surface acoustic waves of a few tens of nanometers wavelength, to study elasticity of very thin isotropic SiC:H films (tens of nanometers thickness).

Therefore, they will not be taken into account in the following discussion. Nevertheless, let us mention that the differences in values regarding the lowest thicknesses are confirmed by the ellipsometry measurements shown in Fig. 9, which tends to prove a sharp difference between the 20 nm sample and the other ones.

Furthermore, let us mention that our setups are able to determine the samples mechanical characteristics down to about 40 nm. As it can be seen in Fig. 8, beyond 40 nm, the longitudinal and transverse velocities, as well as the Young's modulus, tend to decrease when the sample thickness increases, whereas the Poisson's ratio remains stable if we take into account the measurement uncertainty.

Several explanations can be evoked in the case of films with a few tens of nanometers thickness. Among them, the one we considered the most likely to happen is a plausible modification of the influence of the porosity (fraction, pore size, shape, and distribution can be modified) when the film thickness is decreased.[29] We think the films are inhomogeneous along the growth axis as observed in cross section transmission electron micrograph (not shown here) leading to a modification of the effective mechanical properties when varying the film's thickness. In the case of our films, it seems that the porosity influence is less important for the thinner films as the Young's modulus is increasing when the thickness is decreasing approaching the dense bulk reference value of 209 GPa from Pabst *et al.*,[26] in agreement with the measured decrease of the porosity fraction (5%). This is an extrinsic origin while for very thin film (only a few nm thick) out of our sensitivity, the intrinsic mechanical properties can be modified too, due to a change of the local connectivity between atoms.[30]

As before, the Young's modulus can be compared with the value obtained with a nanoindenter regarding a 100 nm thick zirconia sample: $(E_{ZrO2})_{nano} = 140 \pm 5\ GPa$. This time, the discrepancy in values obtained with acoustical methods and with nanoindentation is smaller than in the previous cases (CR39© substrate and anti-abrasion layer), even if the Young's modulus still increases with the measurement

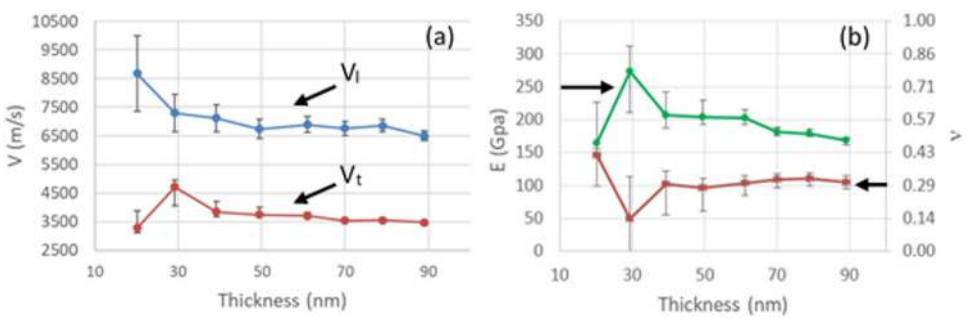

FIG. 8. Mechanical characteristics of zirconia samples as a function of their thickness: longitudinal and transverse velocities (a), Young's modulus, and Poisson's ratio (b).

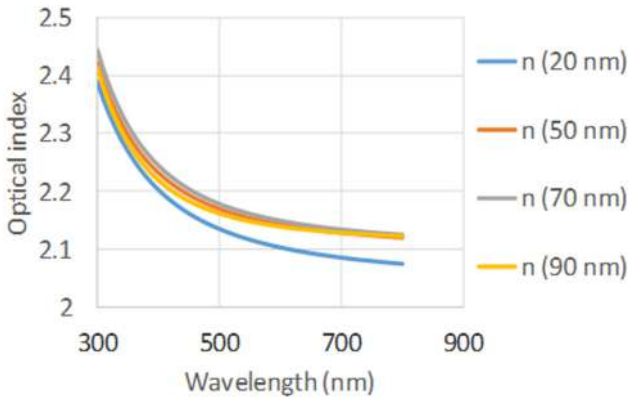

FIG. 9. Ellipsometry measurement of the optical index of zirconia samples as a function of the wavelength. Four sample thicknesses have been investigated: 20 nm, 50 nm, 70 nm, and 90 nm.

frequency. This could be explained by a high value of the zirconia hardness, even for low frequency measurement (i.e., nanoindentation) and the little influence of its viscoelastic properties.

Our approach has been focused on samples deposited on silicon wafer; however, the effect of substrate on the elastic properties can be challenged. Consequently, we have also carried out elastic bilayer characterization using ZrO_2 (80 nm)/SiOCH (80 nm) deposited on a CR39© polymer substrate with a hardcoating. Measurements performed on such structures did not reveal significant changes in sound velocities compared to their counterparts on silicon wafer.

These results pave the way to the study of the elasticity in a complete ophthalmic lens including the entire stack.

IV. CONCLUSIONS AND PROSPECTS

In this paper, optical layers have been studied thanks to two complementary acoustical methods: Picosecond Ultrasonics and Brillouin Light Scattering. First, each layer has been considered separately, the two methods giving the longitudinal and transverse velocities, all the elastic coefficients, the Young's modulus, and the Poisson's ratio of the layer. These physical quantities have thus been obtained regarding the CR39© substrate, the anti-shock layer, the anti-abrasion layer, and the two components of an anti-reflective coating (zirconia and silica). Finally, a deeper study on the zirconia led to two interesting results: the two acoustical techniques proved the zirconia to be isotropic in the two studied geometries (in plane and out of plane); also, considering thin zirconia samples (down to about 40 nm concerning reliable results), the zirconia stiffness tends to increase when the thickness decreases. This stiffening is revealing the heterogenous microstructure as a function of the thickness, for the porosity is lowered for thinner films. We also mentioned in this paper the results obtained, thanks to a nanoindenter showing different values of the Young's modulus compared to acoustical methods. Further analysis could be helpful to investigate in a wider range, the influence of the frequency in relation with its influence on the viscoelastic properties.

ACKNOWLEDGMENTS

The authors would like to thank the help obtained from the LABEX MATISSE and the LABEX SEAM (Nos. ANR-11-LABX-086 and ANR-11-IDEX-0005-02) for their contribution in this project gathering INSP (UPMC University), LSPM (Paris XIII University), and Essilor.

[1]M. Mildebrath and K. Klemm, Int. Soc. Opt. Photonics **6403**, 64030W (2007).
[2]F. Samson, Surf. Coatings Technol. **81**(1), 79 (1996).
[3]R. Long and L. D. Martin, J. Appl. Phys. **115**(23), 233514 (2014).
[4]W. C. Oliver and G. M. Pharr, J. Mater. Res. **19**(1), 3 (2004).
[5]D. Mercier, V. Mandrillon, M. Verdier, and Y. Brechet, Matér. Tech. **99**(2), 169 (2011).
[6]J. Hay and B. Crawford, J. Mater. Res. **26**(6), 727 (2011).
[7]I. Stachiv, D. Vokoun, and Y.-R. Jeng, Appl. Phys. Lett. **104**(8), 083102 (2014).
[8]B. C. Daly, S. T. Bailey, R. Sooryakumar, and S. W. King, J. Nanophotonics **7**(1), 073094 (2013).
[9]G. Scarcelli, P. Kim, and S. H. Yun, Biophys. J. **101**(6), 1539 (2011).
[10]P. Vaneeckhoutte, Y. Leclaire, and A. Robert, EP 0614957 B1 (17 September 1997).
[11]P. Roisin and M. Thomas, U.S. patent 8846140 B2 (30 September 2014).
[12]C. Thomsen, J. Strait, Z. Vardeny, H. J. Maris, J. Tauc, and J. J. Hauser, Phys. Rev. Lett. **53**(10), 989 (1984).
[13]F. Xu, L. Belliard, D. Fournier, E. Charron, J.-Y. Duquesne, S. Martin, C. Secouard, and B. Perrin, Thin Solid Films **548**, 366 (2013).
[14]L. Belliard, T. W. Cornelius, B. Perrin, N. Kacemi, L. Becerra, O. Thomas, M. E. Toimil-Molares, and M. Cassinelli, J. Appl. Phys. **114**(19), 193509 (2013).
[15]L. Belliard, A. Huynh, B. Perrin, A. Michel, G. Abadias, and C. Jaouen, Phys. Rev. B **80**(19), 155424 (2009).
[16]C. Thomsen, H. T. Grahn, H. J. Maris, and J. Tauc, Opt.s Com. **60**, 55 (1986).
[17]P. Djemia, C. Dugautier, C. Chauveau, E. Dogheche, M. I. De Barros, and L. Vandelbulcke, J. Appl. Phys. **90**(8), 3771 (2001).
[18]G. Abadias, P. Djemia, and L. Belliard, Surf. Coatings Technol. **257**, 129 (2014).
[19]A. Fillon, C. Jaouen, A. Michel, G. Abadias, C. Tromas, L. Belliard, B. Perrin, and Ph. Djemia, Phys. Rev. B. **88**, 174104 (2013).
[20]P. Djemia, F. Ganot, P. Moch, V. Branger, and P. Goudeau, J. Appl. Phys. **90**(2), 756 (2001).
[21]R. Loudon, Phys. Rev. Lett. **40**, 581 (1978).
[22]D. Faurie, N. Girodon-Boulandet, A. Kaladjian, F. Challali, G. Abadias, and P. Djemia, Rev. Sci. Instrum. **88**(2), 023903 (2017).
[23]P. Djemia, F. Ganot, C. Dugautier, and M. Quilichini, Solid State Commun. **106**(7), 459 (1998).
[24]J. D. Ferry, *Viscoelastic Properties of Polymers*, 3rd ed. (Wiley, New York, 1980).
[25]G. W. Radebaugh and A. P. Simonelli, J. Pharm. Sci. **72**(4), 422 (1983).
[26]W. Pabst, E. Gregorová, and M. Černý, J. Eur. Ceramic Soc. **33**(15-16), 3085 (2013).
[27]P. A. Mante, J. F. Robillard, and A. Devos, Appl. Phys. Lett. **93**(7), 071909 (2008).
[28]G. Ghislotti, C. E. Bottani, P. Mutti, C. Byloos, L. Giovannini, and F. Nizzoli, Phys. Rev. B **51**(15), 9875 (1995).
[29]H. Ogi, T. Shagawa, N. Nakamura, M. Hirao, H. Odaka, and N. Kihara, Phys. Rev. B **78**(13), 134204 (2008).
[30]J. N. Hernandez-Charpak, K. M. Hoogeboom-Pot, Q. Li, T. D. Frazer, J. L. Knobloch, M. Tripp, S. W. King, E. H. Anderson, W. Chao, M. M. Murnane, H. C. Kapteyn, and D. Nardi, Nano Lett. **17**(4), 2178 (2017).